

Cobalt-Based Pyroxenes: A New Playground for Kitaev Physics and Ising Model Realization

Pavel A. Maksimov,^{1,2} Alexey V. Ushakov,² Andey F. Gubkin,^{2,3} Günther J. Redhammer,⁴ Stephen M. Winter,⁵ Alexander I. Kolesnikov,⁶ Antonio M. dos Santos,⁶ Zheng Gai,⁷ Michael A. McGuire,⁸ Andrey Podlesnyak,^{6,*} and Sergey V. Streltsov^{2,9,†}

¹*Bogolyubov Laboratory of Theoretical Physics, Joint Institute for Nuclear Research, Dubna, Moscow region 141980, Russia*

²*M.N. Miheev Institute of Metal Physics of Ural Branch of Russian Academy of Sciences, S. Kovalevskaya St. 18, 620990 Ekaterinburg, Russia*

³*Institute of Natural Sciences and Mathematics, Ural Federal University, Mira St. 19, 620002 Ekaterinburg, Russia*

⁴*Department of Chemistry and Physics of Materials, University of Salzburg, Jakob-Haringer-Strasse 2a, Salzburg A-5020, Austria*

⁵*Department of Physics and Center for Functional Materials, Wake Forest University, NC 27109, USA*

⁶*Neutron Scattering Division, Oak Ridge National Laboratory, Oak Ridge, TN 37831, USA*

⁷*Center for Nanophase Materials Sciences, Oak Ridge National Laboratory, Oak Ridge, TN 37831, USA*

⁸*Materials Science and Technology Division, Oak Ridge National Laboratory, Oak Ridge, TN 37831, USA*

⁹*Department of Theoretical Physics and Applied Mathematics, Ural Federal University, Mira St. 19, 620002 Ekaterinburg, Russia*

(Dated: January 25, 2024)

Recent advances in the study of cobaltites have unveiled their potential as a promising platform for realizing Kitaev physics in honeycomb systems and the Ising model in weakly coupled chain materials. In this manuscript, we explore the magnetic properties of pyroxene $\text{SrCoGe}_2\text{O}_6$ using a combination of neutron scattering, *ab initio* methods, and linear spin-wave theory. Through careful examination of inelastic neutron scattering powder spectra, we propose a modified Kitaev model to accurately describe the twisted chains of edge-sharing octahedra surrounding Co^{2+} ions. The extended Kitaev-Heisenberg model, including a significant anisotropic bond-dependent exchange term with $K/|J| = 0.96$, is identified as the key descriptor of the magnetic interactions in $\text{SrCoGe}_2\text{O}_6$. Furthermore, our heat capacity measurements reveal an effect of an external magnetic field (approximately 13 T) which shifts the system from a fragile antiferromagnetic ordering with $T_N = 9$ K to a field-induced state. We argue that pyroxenes, particularly those modified by substituting Ge with Si and its less extended *p* orbitals, emerge as a novel platform for the Kitaev model. This opens up possibilities for advancing our understanding of Kitaev physics.

INTRODUCTION

Kitaev materials, where strong spin-orbit coupling (SOC) results in a pronounced exchange anisotropy frustrating a magnetic sub-system, have become one of the most actively studied subjects in physics of magnetic materials^{1,2}. This is not only due to the possible realization of a long-sought spin-liquid state and exotic Majorana excitations³, but also since in these materials anisotropic terms of the exchange interaction do manifest themselves in various physical observables such as magnetization⁴⁻⁷, thermal conductivity⁸⁻¹⁰, Raman spectra¹¹⁻¹³ and spin-spin correlations¹⁴⁻¹⁷.

Another important factor affecting magnetic properties is dimensionality. It is well known that the temperature of a long-range magnetic order can be strongly reduced going from 3D to 2D or 1D^{18,19}. One-dimensional magnetic systems represent a limiting and very specific case, where each spin is connected with only two neighbors and no interchain exchange pathways to assist a long-range magnetic order are possible. This leads to a number of unexpected phenomena, including complete suppression of the ordered state, and dependence of the spin excitation spectra on spin-parity with the low-lying excitations very different from standard spin-waves^{20,21}.

It was recently realized that these two intriguing concepts of Kitaev physics and one-dimensionality naturally meet in the case of CoNb_2O_6 ²². This material was considered as a

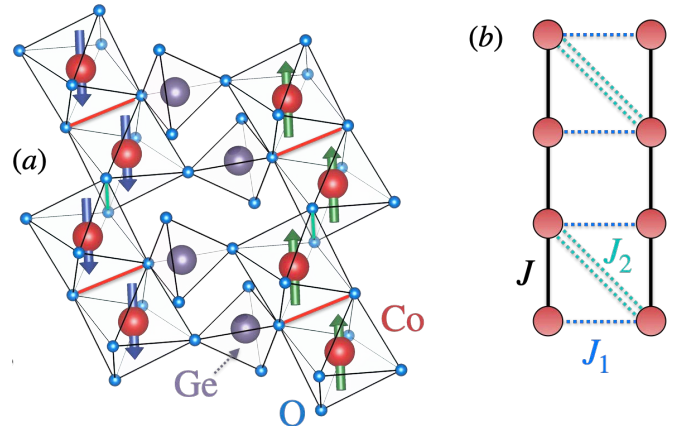


FIG. 1. **Structural details and exchange couplings in $\text{SrCoGe}_2\text{O}_6$.** (a) Crystal structure and experimentally observed magnetic order in $\text{SrCoGe}_2\text{O}_6$. Strontium is not shown for clarity. Two different types of common edges between CoO_6 octahedra are shown by red and green lines. (b) A sketch of the spin sub-lattice: J is intra-chain, J_1 and J_2 are inter-chain exchange parameters. While there are four adjacent chains to each Co-Co chain, only one is shown for clarity. All neighboring chains and the coordinate system are presented in the Methods section.

model system to study quantum criticality in Ising chains²³⁻²⁶. The ground state of Co^{2+} can be described by the effective total momentum $j_{\text{eff}} = 1/2$ as in many other cobaltites, which are under active investigation now²⁷⁻³¹. Moreover, CoO_6 octahedra form zigzag chains sharing their edges. This particular geometry with 90° Co-O-Co bond can lead to the

* Corresponding author: podlesnyakaa@ornl.gov

† Corresponding author: streltsov.s@gmail.com

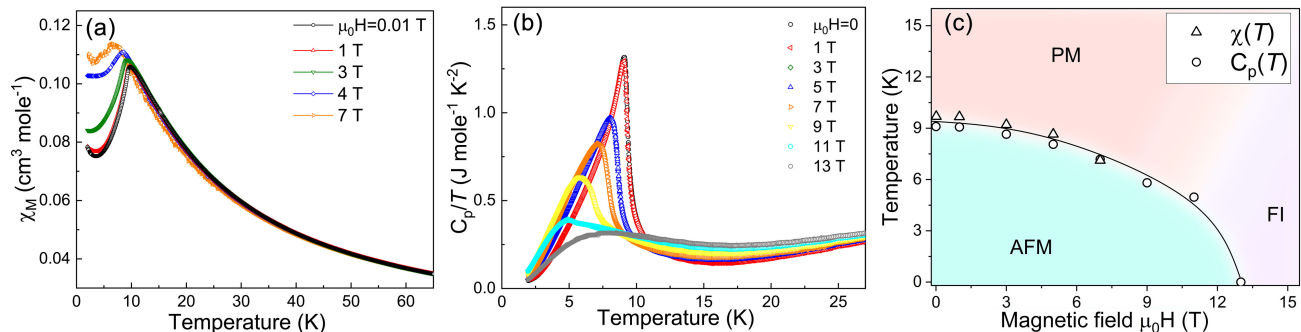


FIG. 2. **Magnetic susceptibility, heat capacity and magnetic phase diagram of SrCoGe₂O₆.** (a) Magnetic susceptibility curves $\chi_M(T)$ of SrCoGe₂O₆ measured in applied magnetic fields after zero-field cooling (ZFC) procedure. (b) Heat capacity curves $C_p(T)/T$ of SrCoGe₂O₆ measured in applied magnetic fields up to $\mu_0H = 13$ T. (c) Magnetic phase diagram of SrCoGe₂O₆ plotted in $T - \mu_0H$ coordinates. PM, FI and AFM mark paramagnetic state, field-induced state, and antiferromagnetic state, respectively.

bond-dependent anisotropy of exchange interactions^{32,33}. Indeed, Ising bond-dependent anisotropy (so-called “twisted Kitaev chain” model) was successfully applied to explain THz spectroscopy measurements²², although the angle between local Ising axes was found to be 34° (rather than the 90° for the ideal Kitaev chain), implying significant uniform Ising anisotropy. As such, an alternative related model, consisting of uniform Ising anisotropy and off-diagonal exchange, has also been used in the literature to describe results of inelastic neutron scattering (INS) experiments^{26,34}. The bond-independent anisotropic exchange arises from the effects of local crystal field distortions on the composition of the $j_{\text{eff}} = 1/2$ moments²⁹, making evaluation of the crystal field terms an important diagnostic of Co²⁺ systems.

In this work, we present the results of INS experiments analyzed by linear spin-wave theory (LSWT) and density functional theory (DFT) calculations of another material consisting of Co zigzag chains - pyroxene SrCoGe₂O₆. Pyroxenes constitute a large class of natural minerals, forming ~ 20 vol% of the Earth’s crust^{35,36}, and various synthetic compositions. There are many pyroxenes with magnetic transition metals such as, e.g., aegirine NaFeSi₂O₆, chinese jade Na(Al,Fe)Si₂O₆, and kosmochlor NaCrSi₂O₆. They were shown to exhibit a variety of intriguing physical properties, such as multiferroicity³⁷, orbital-Peierls^{38–40} or spin-state transition⁴¹, but generally they can be considered as quasi-1D magnets. In pyroxene compounds, the transition metals are octahedrally coordinated with oxygens forming zigzag chains separated by SiO₄ or GeO₄ tetrahedra as shown in Fig. 1(a).

SrCoGe₂O₆ orders magnetically below $T_N = 9$ K with spins coupled ferromagnetically in the chains and antiferromagnetic (AFM) order between chains, see Fig. 1(a)⁴². The effective magnetic moment in Curie-Weiss theory is larger than the spin-only value, which points to a significant orbital contribution. Together with strong magnetic anisotropy⁴², these measurements highlight the importance of spin-orbit physics in SrCoGe₂O₆.

RESULTS

Thermodynamic measurements

We start with magnetic susceptibility data $\chi_M(T)$ measured on a polycrystalline sample of SrCoGe₂O₆ in applied magnetic fields up to $\mu_0H = 7$ T after zero-field cooling (ZFC) procedure (see Fig. 2(a)). All the measured ZFC-curves reveal AFM-like behavior and well-defined anomaly around the Néel temperature similar to the susceptibility data reported in Ref.⁴². The application of an external magnetic field partially suppresses the low-temperature AFM state and shifts the anomaly towards lower temperatures. No sign of saturation was observed on the isothermal magnetization curves $M(H)$ measured at $T = 2$ K in magnetic fields up to 7 T (see Supplementary Note 1 for details).

Similar behavior can be seen in the heat capacity data measured in applied magnetic fields up to $\mu_0H = 13$ T and plotted as a function of temperature $C_p(T)/T$, Fig. 2(b). The Néel temperature of SrCoGe₂O₆ was found to be $T_N = 9.1$ K as a peak of λ -type anomaly in zero magnetic field. On the contrary, no sign of the λ -type anomaly is observed on the $C_p(T)/T$ curve measured in the applied magnetic field $\mu_0H = 13$ T implying complete suppression of the low-temperature AFM state in SrCoGe₂O₆. The field-temperature phase diagram, deduced from the heat capacity and magnetic susceptibility data, is summarized in Fig. 2(c).

Another important information, that thermodynamic measurements provide is the degeneracy of the ground state. By comparing experimental $C_p(T)$ dependence with its non-magnetic analog, it was demonstrated that the magnetic contribution to the specific heat saturates at $R \ln 4$, but one might note that release of the entropy at T_N corresponds to $R \ln 2$ ⁴². This clearly shows that the ground state is a doublet and suggests that the low-lying excitations can be described by $j_{\text{eff}} = 1/2$ due to a sizable SOC despite strong distortions of CoO₆ octahedra.

Inelastic neutron scattering

To demonstrate that the doublet corresponding to the ground state of SrCoGe₂O₆ is well isolated from other states, first

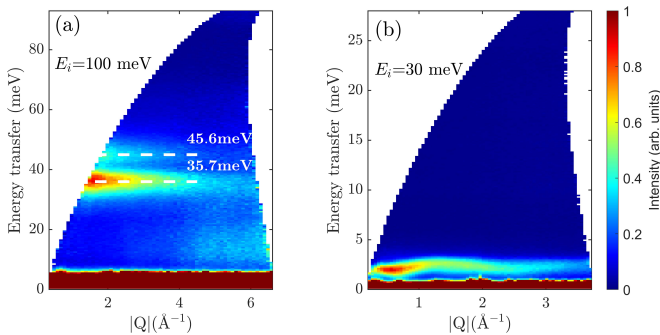


FIG. 3. **High-energy inelastic neutron scattering results.** INS taken at the SEQUOIA spectrometer at $T = 6$ K with incident neutron energies $E_i = 100$ meV (a) and $E_i = 30$ meV (b), displaying CEF excitations in $\text{SrCoGe}_2\text{O}_6$.

we conducted high-energy INS measurements using incident energies $E_i = 30, 100, 150$ and 250 meV (see Supplementary Note 2 for the details of high-energy INS spectra). The INS spectrum, depicted in Fig. 3(a), clearly exhibits two non-dispersive excitations at energy transfers of $35.7(3)$ meV and $45.6(3)$ meV. The intensity of these excitations decreases with increasing momentum transfer, providing definitive evidence that they correspond to ground-state crystal electric field (CEF) transitions of the Co^{2+} ion. Importantly, we did not observe any CEF levels below 30 meV, as illustrated in Fig. 3(b). This finding, along with the complementary heat capacity and susceptibility data presented in Fig. 2, supports the conclusion that the low-temperature magnetic properties of $\text{SrCoGe}_2\text{O}_6$ are primarily governed by the ground-state doublet, which effectively behaves as a $j_{\text{eff}} = 1/2$ pseudospin. The observed CEF levels represent $j_{\text{eff}} = 1/2 \rightarrow 3/2$ excitations, which are split by the distortion of the local crystal field away from ideal octahedral symmetry. Interestingly, in the INS study of another cobaltite CoNb_2O_6 with Co^{2+} ions a very similar level structure was observed with excitation energies ~ 30 and 50 meV and it was successfully explained by a model based on pseudospin $j_{\text{eff}} = 1/2$ ⁴³. However, it is worth noting that the splitting of the $j_{\text{eff}} = 3/2$ levels is significantly smaller in $\text{SrCoGe}_2\text{O}_6$, which points to a potentially reduced effect of bond-independent anisotropies in the magnetic couplings.

Figure 3(b) provides clear evidence of a dispersive spin-wave excitation extending up to approximately 3 meV, indicating significant couplings in $\text{SrCoGe}_2\text{O}_6$. However, the spectra obtained at high incident energies lack the necessary energy resolution to distinguish or resolve these low-energy features adequately. To further investigate the spin dynamics of the Co magnetic sublattice, we conducted measurements on the Cold Neutron Chopper Spectrometer (CNCS) with $E_i = 5.0$ meV at a temperature of 1.7 K.

The experimentally observed low-energy INS as a function of energy and momentum transfer is shown in Fig. 4(a). The excitation spectrum is dominated by a strong dispersive magnon-like mode within the 2 to 3 meV energy range. A second excitation at around 2 meV appears as a dispersionless band with modulated intensity across the entire Q region.

An evident concave shape, exhibiting a minimum around $|Q| \sim 0.7 \text{ \AA}^{-1}$, is observable in the data. This characteristic is reminiscent of the behavior observed in other honeycomb lattice magnets with zigzag AFM order^{44,45}. No magnetic signals were observed above an energy transfer of 3 meV.

First principle calculations

Careful analysis of the INS can be performed within the spin-wave theory, but to reduce the number of model parameters and also narrow their value range we first perform DFT calculations.

$\text{SrCoGe}_2\text{O}_6$ was found to be an insulator with the band gap of 1.8 eV and magnetic moments $2.8 \mu_B$ in GGA+U calculations for Hubbard $U = 6$ eV and Hund's $J_H = 0.9$ eV, typically used in literature³⁰. Account of the SOC via GGA+U+SOC shows that spins are predominantly oriented along c axis and orbital contribution to the magnetic moment is $0.2 \mu_B$.

The spin lattice in pyroxenes can be characterized by chains connected by two inter-chain couplings J_1 and J_2 , see Figs. 1(b) and Methods section. These inter-chain exchanges are mediated via hopping through GeO_4 tetrahedra. Direct calculation of the exchange coupling by the total energy method in GGA+U approach reveals that inter-chain exchanges are $J_1 = 0.67$ meV and $J_2 = 1.40$ meV (AFM), and we estimate intra-chain coupling as $J = 0.08$ meV (AFM). It is worthwhile mentioning that account of the SOC can modify the character of the ground and excited states considerably and therefore affect exchange interactions. Moreover, this type of calculations do not take into account a multiplet structure of excited states, which were shown to be rather important for ‘‘Kitaev’’ cobaltites^{29,46}. While a large inter-chain coupling seems surprising, Ge $4p$ orbitals are known to be rather extended and can substantially increase this interaction⁴⁷. Strong inter-chain exchange implies that long-range order is stable towards fluctuations and spin-wave theory can be used to describe magnetic excitations, instead of spinons such as the case of CoNb_2O_6 ²⁶.

Spin-wave theory

The gapped nature of the magnetic excitation spectrum, as shown in Fig. 4(a), implies that the isotropic Heisenberg model is not enough to describe its properties. Moreover, the spin-orbit entangled structure of the $j_{\text{eff}} = 1/2$ pseudospin allows for anisotropic interactions, given they obey the symmetry of the lattice.

For $\text{SrCoGe}_2\text{O}_6$, similarly to previously studied CoNb_2O_6 ²⁶, the glide symmetry of the zigzag chains and bond inversion symmetry allows for six nearest-neighbor couplings:

$$J^{(m)} = J \begin{pmatrix} J^{xx} & (-1)^m J^{xy} & J^{xz} \\ (-1)^m J^{xy} & J^{yy} & (-1)^m J^{yz} \\ J^{xz} & (-1)^m J^{yz} & J^{zz} \end{pmatrix}, \quad (1)$$

where $m = 1, 2$ corresponds to two types of bonds in the staggered structure of the chains. The corresponding reference frame for spin operators and two types of bonds, denoted by x and y , are shown in the Methods section.

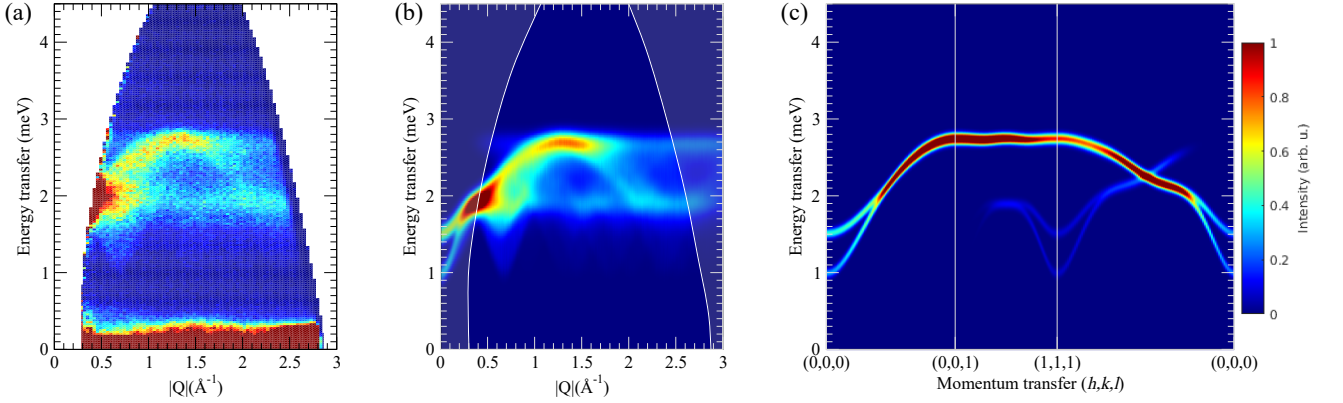


FIG. 4. **Comparison between the experimental and calculated inelastic neutron spectra in SrCoGe₂O₆.** (a) INS data taken at the CNCS spectrometer with incident neutron energy $E_i = 5.0$ meV. (b) Linear spin-wave calculation for the powder averaged spectrum for the best-fit set of parameters, see text. (c) Same, without averaging, along the contour involving high-symmetry points.

Moreover, DFT calculations predict two large inter-chain interactions. Thus, there are eight parameters in the model even without taking into account the anisotropy of J_1 and J_2 . With rather limited information on the powder INS data, the spin-wave fit of the full model becomes extremely challenging. Therefore, it is advisable to consider a simplified model with fewer free parameters, which can still sufficiently fit the inelastic powder data.

We argue that the ground state and spin-wave spectrum of SrCoGe₂O₆ can be described by the one-dimensional version of the extended Kitaev-Heisenberg model

$$\mathcal{H} = \sum_{\langle ij \rangle_\gamma} JS_i \cdot S_j + K S_i^\alpha S_j^\alpha + \Gamma (S_i^\alpha S_j^\beta + S_i^\beta S_j^\alpha) + \Gamma' (S_i^\gamma S_j^\alpha + S_i^\gamma S_j^\beta + S_i^\alpha S_j^\gamma + S_i^\beta S_j^\gamma), \quad (2)$$

where $\{\alpha, \beta, \gamma\} = \{y, z, x\}$ at the x -bond, and $\{z, x, y\}$ at the y -bond. The reasoning for this choice of the exchange model is the fact that the edge-sharing octahedra and staggered zigzag chains can be viewed as a honeycomb model with one leg missing⁴⁸, also referred to as Kitaev spin chain^{22,49-51}. Therefore, we use a four-parameter model for Co chains as an ansatz, which obeys the symmetries of the general Hamiltonian (1), and represents a subset of the full model with parameters being related as

$$\begin{aligned} J_{xx} &= J + \frac{1}{6} (K - 4\Gamma - 2\Gamma'), \\ J_{yy} &= J + K/2 - \Gamma', \\ J_{zz} &= J + \frac{1}{3} (K + 2\Gamma + 4\Gamma'), \\ J_{xy} &= \frac{1}{2\sqrt{3}} (K + 2\Gamma - 2\Gamma'), \\ J_{xz} &= \frac{1}{3\sqrt{2}} (-K + \Gamma - \Gamma'), \\ J_{yz} &= -\frac{1}{\sqrt{6}} (K - \Gamma + \Gamma'). \end{aligned} \quad (3)$$

While we have to acknowledge that it is the full six-parameter

model that needs to be used to describe SrCoGe₂O₆, some properties are naturally described by the extended Kitaev-Heisenberg model. As we show in the Methods section, there is a parameter regime of the intra-chain ferromagnetic state with magnetic moments in the x - z plane, which is the state observed experimentally⁴². We refer to this state as FM- xz , it is illustrated in the Methods section. Thus, fixing spin direction can immediately place constraints on the parameters of the Kitaev-Heisenberg model⁵²:

$$\tan 2\theta = 4\sqrt{2} \frac{1+r}{7r-2}, \quad r = -\frac{\Gamma}{K+\Gamma'}, \quad (4)$$

where $\theta \approx 6^\circ$, according to measurements on SrCoGe₂O₆⁴². However, the anisotropy of g -factors, which is unknown, can modify this value. Moreover, according to DFT calculations, inter-chain couplings are rather large and must be included. Therefore, to provide a reasonable fitting to neutron-scattering data we limit our model for SrCoGe₂O₆ to four intra-chain exchanges and two inter-chain exchanges.

We use LSWT to calculate the magnetic spectrum in the AFM state where chains are ordered ferromagnetically in the FM- xz configuration. Due to the scrambled nature of the neutron scattering on the powder sample, the spin-wave fit may be challenging, especially due to the large parameter phase space. However, there are three discernible features of the spectrum that we can use for the fits of magnon energies, as one can infer from Fig. 4(a): (i) the minimum of intensity at 1 meV and $|\mathbf{Q}| \simeq 0.7 \text{ \AA}^{-1}$; (ii) the flat band at 1.9 meV; (iii) a well-defined maximum at 2.7 meV. By studying spin-wave spectra for various parameter sets we found that the first feature originates in $\mathbf{k} = 0$ mode, as one can see in Fig. 4(c), while 1.9 and 2.7 meV features can be traced to $(1/2, 1/2, 0)$ modes. This simplifies calculations significantly since these magnon energies can be obtained analytically, see Methods section.

Thus, we can use a combination of three criteria for magnon energies from neutron-scattering data and the tilt angle (4) to use for the analytical fitting of four criteria of the intra-chain exchange matrix. We keep inter-chain exchanges as free pa-

rameters, and for each set of (J_1, J_2) we obtain (J, K, Γ, Γ') from fitting analytical expressions to the four criteria above. Next, we scan through the $J_1 - J_2$ phase space and obtain the dynamical structure factor using SpinW package⁵³ to compare to the CNCS neutron-scattering data. During the calculation, a Gaussian broadening with $\sigma = 0.2$ meV was applied. The result is shown in Fig. 5 as an intensity plot of fit quality

$$\chi = \sum_{Q, \omega} (\mathcal{S}^{\text{exp}}(Q, \omega) - \mathcal{S}^{\text{calc}}(Q, \omega))^2. \quad (5)$$

Note that for some parameter sets the ground state is not FM- xz relevant to SrCoGe₂O₆, according to classical minimization but instead spiral or FM- y (shown in Fig. 7) state, which we also use to limit parameters applicable to SrCoGe₂O₆. According to the definition above the best fit to the powder scattering data is given by the minimum of the fit quality χ in Fig. 5, where χ is normalized to the minimum and maximum values. The best-fit parameter set is obtained with $J_1 = 0.4$ meV and $J_2 = 0.6$ meV. The optimal intra-chain exchanges for these values of inter-chain interactions are given by

$$J = -0.87, K = 0.83, \Gamma = 0.43, \Gamma' = -0.26 \text{ (meV)} \quad (6)$$

The spin-wave calculation for this set of parameters is shown in Fig. 4 with powder averaged signal shown in (b), and the dynamical structure factor along a contour in the BZ in (c). One can see that this parameter set provides an excellent agreement with CNCS data in Fig. 4(a). As an illustration of the quality of the fit, in Fig. 5, right panel, we plot one-dimensional cuts of the spin-spin correlation function for several values of $|\mathbf{Q}|$, together with experimental data. We plot these cuts for three sets of parameters, the optimal ones (blue lines) and two more, shown with orange and green lines. The optimal parameter set matches neutron-scattering data excellently, except for some discrepancy at low energies and small $|\mathbf{Q}|$. We should note that the optimized J_1 and J_2 do not completely agree with DFT predictions, but the ratio of J_2/J_1 is very similar.

DISCUSSION

While Kitaev bond-dependent anisotropic exchange interaction naturally appears in the shared-edge geometry^{32,33}, we would like to stress that the choice of the Kitaev-Heisenberg model as an ansatz for SrCoGe₂O₆ is not unique.

Interestingly, the matrix of the Kitaev-Heisenberg model in the local quantization axes for the best-fit parameters (6) has off-diagonal term J^{xy} (the only off-diagonal term contributing linear spin-wave spectrum) smaller than diagonal terms:

$$\hat{\mathbf{J}}^{\text{loc}} = \begin{pmatrix} -0.65 \mp 0.13 & 0 & \\ \mp 0.13 & -0.19 \pm 0.63 & \\ 0 & \pm 0.63 & -0.93 \end{pmatrix} \text{ (meV)}. \quad (7)$$

The fact that off-diagonal terms J^{xy} are smaller than diagonal ones motivated us to study an alternative model where we neglect small off-diagonal terms and come to an XYZ Hamiltonian in the local coordinate systems with three independent parameters: J^{xx} , J^{yy} , and J^{zz} . In this case, the direction of

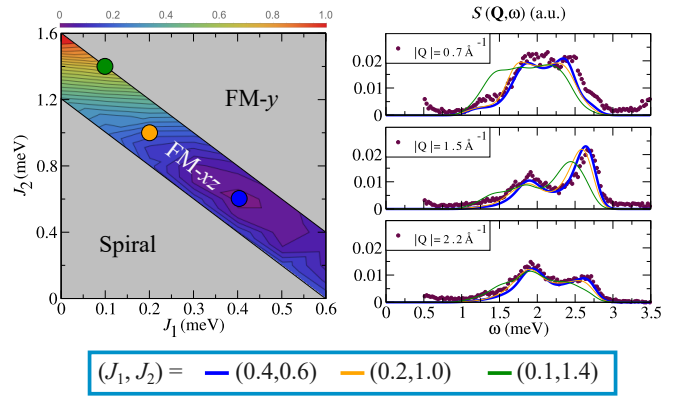


FIG. 5. **Determination of exchange interactions in SrCoGe₂O₆ from neutron scattering data.** (left) Fit quality, shown as a function of the inter-chain parameters J_1 and J_2 [Fig. 1(b)], see text. The blue dot indicates the position of the global minimum. (right) Constant- Q cuts through the experimental (symbols) and calculated (solid lines) spectral functions for three representative Q values.

spins is determined, not by anisotropic exchanges but by the distortions of the lattice and subsequent rotation of quantization axes²⁹.

We have also performed spin-wave calculations for this model and the best-fit powder spectrum provides a satisfactory agreement with neutron scattering data, albeit still slightly worse than the Kitaev-Heisenberg model. This fact implies that the exchange matrix for SrCoGe₂O₆ is most likely close to the diagonal-only model but off-diagonal terms J^{xy} are non-negligible and improve the fitting of neutron-scattering data. Moreover, smaller splitting of CEF levels in SrCoGe₂O₆, as shown in Fig. 3, compared to CoNb₂O₆⁴³, points to proximity to the cubic limit and the relevance of Kitaev-Heisenberg interactions in SrCoGe₂O₆, instead of Ising model.

In summary, we successfully synthesized powder samples of SrCoGe₂O₆, and performed a detailed study of magnetic excitations by the inelastic neutron scattering, which were analyzed by a combination of *ab initio* and spin-wave theory calculations. These results demonstrate substantial bond-dependent Kitaev exchange, $K/|J| = 0.96$, while our heat capacity measurements revealed that the external magnetic field of ~ 13 T transforms a fragile antiferromagnetic ordering with $T_{\text{CW}} \approx 9$ K to a field-induced state widely discussed in context of Kitaev physics in other cobaltites⁵⁴⁻⁵⁷. Thus, our study demonstrated that pyroxenes can be considered as a new platform for the Kitaev model and, moreover, these materials can be made more one-dimensional changing Ge by Si with less extended p orbitals. This can open up even more exciting perspectives for Kitaev physics.

METHODS

Sample synthesis

Polycrystalline powder of SrCoGe₂O₆ was prepared as a 10 g batch from a stoichiometric mixture of SrCO₃, Co₃O₄ and GeO₂. Starting materials were carefully homogenized by

grinding for 20 minutes under isopropanol in an agate mortar, pressed to pellets and heated in open platinum crucibles in a chamber furnace at a temperature of 1473 K over a period of 21 days with four intermediate regrinding until phase pure and a good crystalline sample was obtained. Phase purity was checked by powder x-ray diffraction using a PANalytical X'Pert Pro MPD equipped with an X'Celerator solid-state detector (for details, see Supplementary Note 3).

Magnetization and heat capacity

For magnetization measurements, 24.6 mg of $\text{SrCoGe}_2\text{O}_6$ were loaded on a Quantum Design MPMS 3 magnetometer. The sample was contained in weight paper and affixed with Apiezon M grease. Temperature-dependent magnetization data were collected under zero-field cooling conditions and sweep mode at several fields (100 Oe and 1, 3, 5, 7 T) from 2 K to 100 K. Companion measurements were performed at 100 Oe and 7 T under settle between 2 K and 50 K every 1 K mode to check for temperature stability. Magnetization under a magnetic field was collected on the same sample on a single quadrant, with increasing field up to 7 T and at several temperatures (2, 10 and 50 K).

Heat capacity was measured using a Quantum Design Physical Property Measurement System. The $\text{SrCoGe}_2\text{O}_6$ powder was mixed with silver powder in equal parts by mass and pressed into a thin pellet. The pellet was cut with a razor blade to produce a 6.08 mg sample that was mounted using Apiezon N-grease for the heat capacity measurement. The heat capacity of the $\text{SrCoGe}_2\text{O}_6$ sample was determined by subtraction of the measured heat capacity data for silver from the total.

Inelastic neutron scattering

INS measurements were performed with the use of the Cold Neutron Chopper Spectrometer CNCS^{58,59} and the Fine Resolution Chopper Spectrometer SEQUOIA⁶⁰ at the Spallation Neutron Source (SNS) at Oak Ridge National Laboratory. A powder sample of $\text{SrCoGe}_2\text{O}_6$ was loaded in an aluminum can for the measurements and a standard orange cryostat was used to cover the temperature region from 1.7 K to 100 K at CNCS, and bottom-loading closed cycle refrigerator ($T = 5.5$ K) at SEQUOIA. Data were collected using fixed incident neutron energies of 250, 150, 100, and 30 meV for SEQUOIA, and 5.0 meV for CNCS. In these configurations, a full width at half maximum (FWHM) resolution of 18, 10, 6.1, and 1.0 meV (SEQUOIA), and 0.15 meV (CNCS) was obtained at the elastic position. For data reduction and analysis we used the MANTID⁶¹ and DAVE⁶² software packages.

DFT+U calculations

The *ab initio* band structure calculations of $\text{SrCoGe}_2\text{O}_6$ were carried out within the framework of density functional theory realized in VASP package⁶³. We used the generalized gradient approximation (GGA)⁶⁴ and projector augmented wave (PAW) method⁶⁵. The exchange-correlation functional in Perdew-Burker-Ernzerhof (PBE) form was applied⁶⁶. The cutoff energy was chosen to be 600 eV and a grid of $4 \times 4 \times 4$ points was used for integration over the Brillouin zone.

The correlation effects were taken into account via GGA+U approach⁶⁷. We chose the onsite Coulomb repulsion parameter to be $U = 6$ eV and Hund's rule coupling parameter was taken as $J_H = 0.9$ eV as typically used in literature for Co ions. The occupation numbers of Co-3d states were obtained by integration within an atomic sphere with a radius 1.302 Å.

Model conventions and spin-wave theory

In general, bilinear exchange Hamiltonian can be represented in a matrix form

$$\hat{\mathcal{H}} = \sum_{\langle ij \rangle} \mathbf{S}_i^T \hat{\mathbf{J}}_{ij} \mathbf{S}_j, \quad (8)$$

where $\hat{\mathbf{J}}_{ij}$ is a 3×3 matrix and can depend on the site position, such as the matrix of the model (1) being different on x and y bonds. If the exchange matrix $\hat{\mathbf{J}}_{ij}$ is not isotropic Heisenberg interaction, then its elements become reference frame dependent.

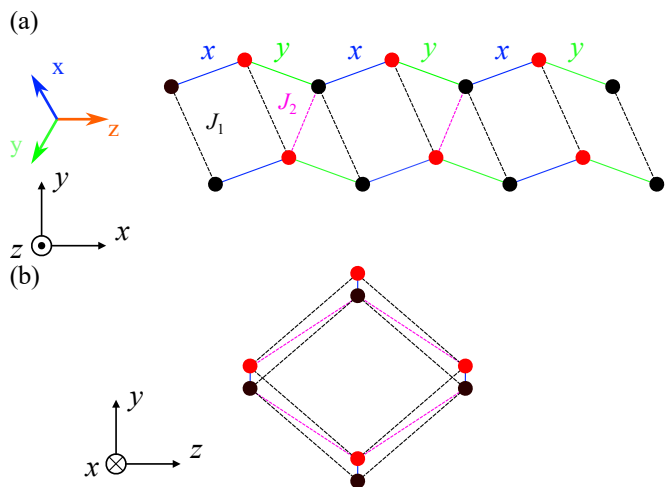


FIG. 6. **Schematic illustration of the exchange Hamiltonian (10).** Due to the staggered structure of Co-chains, there are two types of intra-chain bonds: x and y . Two inter-chain exchanges are allowed due to the exchange paths through Ge ions.

For instance, the extended Kitaev-Heisenberg model (2) is written in cubic axes $\{x, y, z\}$, which are defined by the ideal ligand octahedra of cobalt-oxygen bonds, shown in Fig. 6(a). However, it is also beneficial to represent this model in the crystallographic reference frame $\{x, y, z\}$, also shown in Fig. 6(a). The transformation from cubic to crystallographic axes is given by $\hat{\mathbf{J}}_{\alpha}^{\text{cryst}} = \hat{\mathbf{R}}_c^{-1} \hat{\mathbf{J}}_{\alpha}^{\text{cubic}} \hat{\mathbf{R}}_c$, where $\mathbf{S}_{\text{cubic}} = \hat{\mathbf{R}}_c \mathbf{S}_{\text{cryst}}$, and

$$\hat{\mathbf{R}}_c = \begin{pmatrix} \frac{1}{\sqrt{6}} & -\frac{1}{\sqrt{2}} & \frac{1}{\sqrt{3}} \\ \frac{1}{\sqrt{6}} & \frac{1}{\sqrt{2}} & \frac{1}{\sqrt{3}} \\ -\frac{1}{\sqrt{6}} & 0 & \frac{1}{\sqrt{3}} \end{pmatrix}. \quad (9)$$

Using the transformation above, we yield the extended Kitaev-Heisenberg model in the crystallographic reference

frame as

$$\begin{aligned} \mathcal{H}_{\text{cryst}} = & \sum_{\langle ij \rangle} J_{\text{iso}} \left(S_i^x S_j^x + S_i^y S_j^y + \Delta S_i^z S_j^z \right) \\ & - 2J_{\pm\pm} \left(\left(S_i^x S_j^x - S_i^y S_j^y \right) c_\alpha - \left(S_i^x S_j^y + S_i^y S_j^x \right) s_\alpha \right) \\ & - J_{z\pm} \left(\left(S_i^x S_j^z + S_i^z S_j^x \right) c_\alpha + \left(S_i^y S_j^z + S_i^z S_j^y \right) s_\alpha \right), \end{aligned} \quad (10)$$

where $c_\alpha(s_\alpha) = \cos(\sin)\varphi_\alpha$, here bond-dependent phases are $\varphi_x = 2\pi/3$, $\varphi_y = -2\pi/3$. Note that it contains bond-isotropic XXZ part and two-bond-dependent exchanges. These exchanges are related to the extended Kitaev-Heisenberg model via

$$\begin{aligned} J_{\text{iso}} &= J + \frac{1}{3}(K - \Gamma - 2\Gamma'), \\ \Delta J_{\text{iso}} &= J + \frac{1}{3}(K + 2\Gamma + 4\Gamma'), \\ 2J_{\pm\pm} &= \frac{1}{3}(-K - 2\Gamma + 2\Gamma'), \\ \sqrt{2}J_{z\pm} &= \frac{1}{3}(2K - 2\Gamma + 2\Gamma'), \end{aligned} \quad (11)$$

Phase diagram of the model (10), obtained using Luttinger-Tisza method⁶⁸ is shown in Fig. 7. Note that inter-chain interactions are not included here. We plot slices of the phase space for $J_{\text{iso}} < 0$ at fixed Δ . For large $|J_{\pm\pm}|$ we observe incommensurate spiral states, while for smaller $|J_{\pm\pm}|$ there are two ferromagnetic states. In 'FM- y ' state the spins point along the y -axis, perpendicular to the chain direction. In the 'FM- xz ' state magnetic moments lie in the $x-z$ plane being canted out of the $x-y$ plane at an angle

$$\tan 2\theta = \frac{J_{z\pm}}{J_{\text{iso}}(1 - \Delta) + J_{\pm\pm}}, \quad (12)$$

which we also indicate in the phase diagram. These states are illustrated in Fig. 7. FM- xz state is the one that is observed in experiments on SrCoGe₂O₆⁴². Thus, when extracting parameters for SrCoGe₂O₆ we also check that the exchanges yield the correct ground state.

Using Holstein-Primakoff transformation

$$S_i^+ = \sqrt{2S}a_i, S_i^z = S - a_i^\dagger a_i \quad (13)$$

and standard spin-wave theory calculations we obtain energies at the $\mathbf{k} = 0$ and $\mathbf{k} = (1/2, 1/2, 0)$, which can be expressed analytically:

$$\begin{aligned} \varepsilon_1(0) &= \sqrt{(A - B)^2 - (C + D + F)^2} \\ \varepsilon_2(0) &= \sqrt{(A + B)^2 - (-C + D + F)^2} \\ \varepsilon_3(0) &= \sqrt{(A + B)^2 - (C + D - F)^2} \\ \varepsilon_4(0) &= \sqrt{(A - B)^2 - (C - D + F)^2} \end{aligned} \quad (14)$$

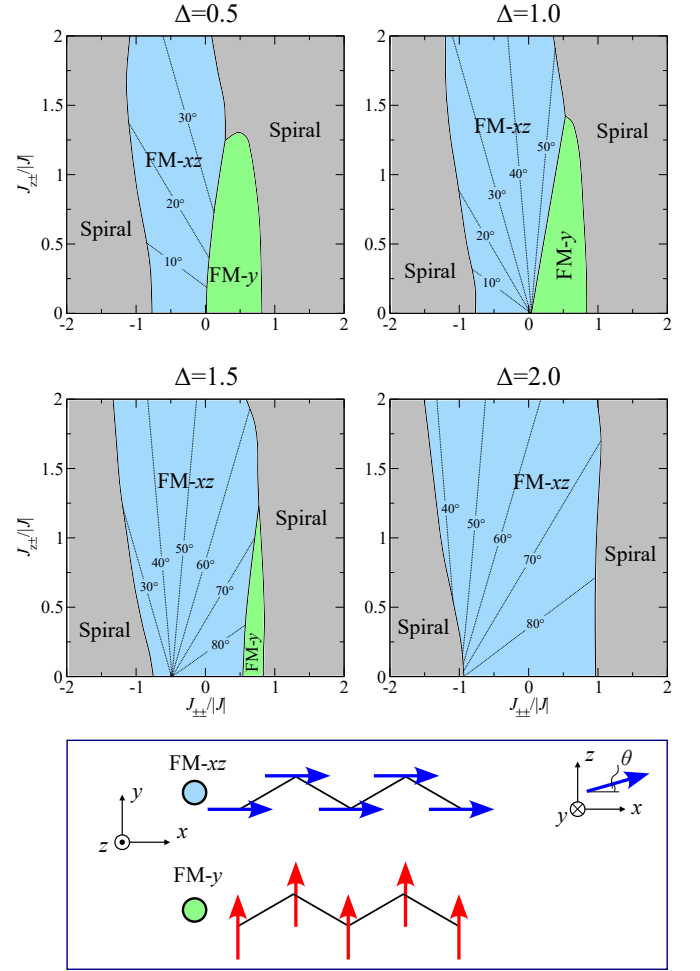


FIG. 7. Classical phase diagrams of the model (10) for various XXZ anisotropy Δ with the structure of the ferromagnetic states. FM- y is the ferromagnetic ordered state with magnetic moments along the y -axis, shown in Fig. 6. FM- xz state is a ferromagnetic ordered state where magnetic moments are in the $x-z$ plane. The angle of canting from the $x-y$ plane is shown on the phase diagrams.

$$\varepsilon_1(1/2, 1/2, 0) = \sqrt{(A - B)^2 - D^2} \quad (15)$$

$$\varepsilon_2(1/2, 1/2, 0) = \sqrt{(A + B)^2 - D^2}$$

where

$$\begin{aligned} A &= -2J^{zz} + 4J_1 + 2J_2 \\ B &= -(J^{xx} + J^{yy}) \\ C &= 4J_1 \\ D &= -(J^{xx} - J^{yy}) \\ F &= 2J_2. \end{aligned} \quad (16)$$

The $J^{\alpha\beta}$ are elements of the exchange matrix \hat{J}_{ij} in the local reference frame of the FM- xz state, which contribute to linear

spin-wave theory:

$$\begin{aligned}
 J^{xx} &= J_{\text{iso}} (\sin^2 \theta + \Delta \cos^2 \theta) + J_{\pm\pm} \sin^2 \theta - \frac{J_{z\pm}}{2} \sin 2\theta \\
 J^{yy} &= J_{\text{iso}} - J_{\pm\pm} \\
 J^{zz} &= J_{\text{iso}} (\cos^2 \theta + \Delta \sin^2 \theta) + J_{\pm\pm} \cos^2 \theta + \frac{J_{z\pm}}{2} \sin 2\theta.
 \end{aligned}
 \tag{17}$$

The expressions above are used to extract exchanges using constraints:

$$\begin{aligned}
 \varepsilon_1(0) &= 1.0 \text{ meV}, \\
 \varepsilon_1(1/2, 1/2, 0) &= 1.9 \text{ meV}, \\
 \varepsilon_2(1/2, 1/2, 0) &= 2.7 \text{ meV}.
 \end{aligned}
 \tag{18}$$

Thus, for a fixed set of inter-chain exchanges (J_1, J_2), the

constraints above, together with the constraint on the tilt angle (12) allows the extraction of the four exchanges of the model (10). Linear transformation (11) yields the exchanges of the Kitaev-Heisenberg model (2).

DATA AVAILABILITY

The datasets generated during the current study are available under the following publicly accessible digital object identifiers (DOI) on the ONCat platform of Oak Ridge National Laboratory, <https://doi.org/10.14461/oncat.data.6541161d1f3c8fcc291bc2df/2204019> and <https://doi.org/10.14461/oncat.data.64d649ab9a4f9cddec92b19a/2204020> for the CNCS and SEQUOIA, respectively.

CODE AVAILABILITY

The code that supports the findings of this study is available from the corresponding author upon reasonable request.

-
- [1] Trebst, S. *Kitaev Materials* (Forschungszentrum Jülich, 2017).
- [2] Takagi, H., Takayama, T., Jackeli, G., Khaliullin, G. & Nagler, S. E. Concept and Realization of Kitaev Quantum Spin Liquids. *Nat. Rev. Phys.* **1**, 264–280 (2019). URL <http://dx.doi.org/10.1038/s42254-019-0038-2>.
- [3] Kitaev, A. Anyons in an exactly solved model and beyond. *Ann. Phys.* **321**, 2–111 (2006). URL <http://www.sciencedirect.com/science/article/pii/S0003491605002381>.
- [4] Kubota, Y., Tanaka, H., Ono, T., Narumi, Y. & Kindo, K. Successive magnetic phase transitions in α -RuCl₃: XY-like frustrated magnet on the honeycomb lattice. *Phys. Rev. B* **91**, 094422 (2015). URL <https://link.aps.org/doi/10.1103/PhysRevB.91.094422>.
- [5] Janssen, L., Andrade, E. C. & Vojta, M. Honeycomb-Lattice Heisenberg-Kitaev Model in a Magnetic Field: Spin Canting, Metamagnetism, and Vortex Crystals. *Phys. Rev. Lett.* **117**, 277202 (2016). URL <https://link.aps.org/doi/10.1103/PhysRevLett.117.277202>.
- [6] Das, S. D. *et al.* Magnetic anisotropy of the alkali iridate Na₂IrO₃ at high magnetic fields: Evidence for strong ferromagnetic Kitaev correlations. *Phys. Rev. B* **99**, 081101 (2019). URL <https://link.aps.org/doi/10.1103/PhysRevB.99.081101>.
- [7] Maksimov, P. A. & Chernyshev, A. L. Easy-plane anisotropic-exchange magnets on a honeycomb lattice: Quantum effects and dealing with them. *Phys. Rev. B* **106**, 214411 (2022). URL <https://link.aps.org/doi/10.1103/PhysRevB.106.214411>.
- [8] Kasahara, Y. *et al.* Unusual Thermal Hall Effect in a Kitaev Spin Liquid Candidate α -RuCl₃. *Phys. Rev. Lett.* **120**, 217205 (2018). URL <https://link.aps.org/doi/10.1103/PhysRevLett.120.217205>.
- [9] Cookmeyer, J. & Moore, J. E. Spin-wave analysis of the low-temperature thermal Hall effect in the candidate Kitaev spin liquid α -RuCl₃. *Phys. Rev. B* **98**, 060412 (2018). URL <https://link.aps.org/doi/10.1103/PhysRevB.98.060412>.
- [10] Hentrich, R. *et al.* High-field thermal transport properties of the Kitaev quantum magnet α -RuCl₃: Evidence for low-energy excitations beyond the critical field. *Phys. Rev. B* **102**, 235155 (2020). URL <https://link.aps.org/doi/10.1103/PhysRevB.102.235155>.
- [11] Sandilands, L. J., Tian, Y., Plumb, K. W., Kim, Y.-J. & Burch, K. S. Scattering Continuum and Possible Fractionalized Excitations in α -RuCl₃. *Phys. Rev. Lett.* **114**, 147201 (2015). URL <https://link.aps.org/doi/10.1103/PhysRevLett.114.147201>.
- [12] Wulferding, D. *et al.* Magnon bound states versus anyonic Majorana excitations in the Kitaev honeycomb magnet α -RuCl₃. *Nat. Commun.* **11**, 1603 (2020). URL <https://doi.org/10.1038/s41467-020-15370-1>.
- [13] Sahasrabudhe, A., Kaib, D. A. S., Reschke, S. *et al.* High-field quantum disordered state in α -RuCl₃: Spin flips, bound states, and multiparticle continuum. *Phys. Rev. B* **101**, 140410 (2020). URL <https://link.aps.org/doi/10.1103/PhysRevB.101.140410>.
- [14] Choi, S. K. *et al.* Spin Waves and Revised Crystal Structure of Honeycomb Iridate Na₂IrO₃. *Phys. Rev. Lett.* **108**, 127204 (2012). URL <https://link.aps.org/doi/10.1103/PhysRevLett.108.127204>.
- [15] Winter, S. M. *et al.* Breakdown of magnons in a strongly spin-orbital coupled magnet. *Nat. Commun.* **8**, 1152 (2017). URL <https://doi.org/10.1038/s41467-017-01177-0>.
- [16] Banerjee, A. *et al.* Excitations in the field-induced quantum spin liquid state of α -RuCl₃. *npj Quantum Mater.* **3**, 8 (2018). URL <https://doi.org/10.1038/s41535-018-0079-2>.
- [17] Kim, J. *et al.* Dynamic Spin Correlations in the Honeycomb Lattice Na₂IrO₃ Measured by Resonant Inelastic x-Ray Scattering. *Phys. Rev. X* **10**, 021034 (2020). URL <https://link.aps.org/doi/10.1103/PhysRevX.10.021034>.
- [18] Mermin, N. D. & Wagner, H. Absence of ferromagnetism or antiferromagnetism in one- or two-dimensional isotropic heisenberg models. *Phys. Rev. Lett.* **17**, 1133–1136 (1966). URL <https://link.aps.org/doi/10.1103/PhysRevLett.17.1133>.
- [19] Katanin, A. A. & Irkhin, V. Y. Magnetic order and spin fluctu-

- ations in low-dimensional insulating systems. *Physics-Usppekhi* **50**, 613 (2007). URL <https://dx.doi.org/10.1070/PU2007v050n06ABEH006313>.
- [20] Haldane, F. D. M. Nonlinear Field Theory of Large-Spin Heisenberg Antiferromagnets: Semiclassically Quantized Solitons of the One-Dimensional Easy-Axis Néel State. *Phys. Rev. Lett.* **50**, 1153–1156 (1983). URL <https://link.aps.org/doi/10.1103/PhysRevLett.50.1153>.
- [21] Faddeev, L. & Takhtajan, L. What is the spin of a spin wave? *Phys. Lett. A* **85**, 375–377 (1981). URL <https://www.sciencedirect.com/science/article/pii/0375960181903352>.
- [22] Morris, C. M., Desai, N., Viirok, J. *et al.* Duality and domain wall dynamics in a twisted kitaev chain. *Nat. Phys.* **17**, 832 (2021). URL <https://doi.org/10.1038/s41567-021-01208-0>.
- [23] Coldea, R. *et al.* Quantum criticality in an Ising chain: experimental evidence for emergent E_8 symmetry. *Science* **327**, 177–180 (2010). URL <https://www.science.org/doi/abs/10.1126/science.1180085>.
- [24] Lee, S., Kaul, R. K. & Balents, L. Interplay of quantum criticality and geometric frustration in columbite. *Nat. Phys.* **6**, 702–706 (2010). URL <https://doi.org/10.1038/nphys1696>.
- [25] Kinross, A. W. *et al.* Evolution of Quantum Fluctuations Near the Quantum Critical Point of the Transverse Field Ising Chain System CoNb_2O_6 . *Phys. Rev. X* **4**, 031008 (2014). URL <https://link.aps.org/doi/10.1103/PhysRevX.4.031008>.
- [26] Fava, M., Coldea, R. & Parameswaran, S. A. Glide symmetry breaking and Ising criticality in the quasi-1D magnet CoNb_2O_6 . *PNAS* **117**, 25219 (2020). URL <https://www.pnas.org/doi/abs/10.1073/pnas.2007986117>.
- [27] Zhong, R., Gao, T., Ong, N. P. & Cava, R. J. Weak-field induced nonmagnetic state in a Co-based honeycomb. *Sci. Adv.* **6**, eaay6953 (2020). URL <https://www.science.org/doi/abs/10.1126/sciadv.aay6953>.
- [28] Elliot, M. *et al.* Visualization of Isospin Momentum Texture of Dirac Magnons and Excitons in a Honeycomb Quantum Magnet. *arXiv: Strongly Correlated Electrons* (2020). URL <https://api.semanticscholar.org/CorpusID:220404640>.
- [29] Winter, S. M. Magnetic couplings in edge-sharing high-spin d^7 compounds. *Journal of Physics: Materials* **5**, 045003 (2022). URL <https://dx.doi.org/10.1088/2515-7639/ac94f8>.
- [30] Maksimov, P. *et al.* Ab initio guided minimal model for the “Kitaev” material $\text{BaCo}_2(\text{AsO}_4)_2$: Importance of direct hopping, third-neighbor exchange, and quantum fluctuations. *Phys. Rev. B* **106**, 165131 (2022). URL <https://link.aps.org/doi/10.1103/PhysRevB.106.165131>.
- [31] Vavilova, E. *et al.* Magnetic phase diagram and possible Kitaev-like behavior of the honeycomb-lattice antimonate $\text{Na}_3\text{Co}_2\text{SbO}_6$. *Phys. Rev. B* **107**, 054411 (2023). URL <https://link.aps.org/doi/10.1103/PhysRevB.107.054411>.
- [32] Liu, H. & Khaliullin, G. Pseudospin exchange interactions in d^7 cobalt compounds: Possible realization of the Kitaev model. *Phys. Rev. B* **97**, 014407 (2018). URL <https://link.aps.org/doi/10.1103/PhysRevB.97.014407>.
- [33] Sano, R., Kato, Y. & Motome, Y. Kitaev-Heisenberg Hamiltonian for high-spin d^7 Mott insulators. *Phys. Rev. B* **97**, 014408 (2018). URL <https://link.aps.org/doi/10.1103/PhysRevB.97.014408>.
- [34] Woodland, L. *et al.* Excitations of quantum Ising chain CoNb_2O_6 in low transverse field: quantitative description of bound states stabilized by off-diagonal exchange and applied field. *arXiv preprint arXiv:2306.01948* (2023). URL <https://arxiv.org/pdf/2306.01948>.
- [35] Deer, W., Howie, R. & Zussman, J. *Rock-Forming Minerals: Single-chain Silicates, Volume 2A*. Rock-Forming Minerals (Geological Society, 1997). URL https://books.google.ru/books?id=x0_kPGjeYcMC.
- [36] Ringwood, A. Role of the transition zone and 660 km discontinuity in mantle dynamics. *Phys. Earth Planet. Inter.* **86**, 5–24 (1994). URL <https://www.sciencedirect.com/science/article/pii/0031920194050589>.
- [37] Jodlauk, S. *et al.* Pyroxenes: a new class of multiferroics. *J. Phys.: Cond. Matter* **19**, 432201 (2007). URL <https://dx.doi.org/10.1088/0953-8984/19/43/432201>.
- [38] Wezel, J. V. & Brink, J. V. D. Orbital-assisted Peierls state in $\text{NaTiSi}_2\text{O}_6$. *EPL* **75**, 957 (2006). URL <http://stacks.iop.org/0295-5075/75/i=6/a=957?key=crossref.812c85f9fecf12539485aabfcbbaeb35>.
- [39] Streltsov, S. V., Popova, O. A. & Khomskii, D. I. Comment on “Sodium Pyroxene $\text{NaTiSi}_2\text{O}_6$: Possible Haldane Spin-1 Chain System”. *Phys. Rev. Lett.* **96**, 249701 (2006). URL <https://link.aps.org/doi/10.1103/PhysRevLett.96.249701>.
- [40] Bozin, E. S. *et al.* Local orbital degeneracy lifting as a precursor to an orbital-selective peierls transition. *Nat. Commun.* **10**, 3638 (2019). URL <http://dx.doi.org/10.1038/s41467-019-11372-w>.
- [41] Streltsov, S. V. & Skorikov, N. A. Spin-state transitions in $\text{CaFeSi}_2\text{O}_6$ and $\text{NaFeSi}_2\text{O}_6$ under pressure. *Phys. Rev. B* **83**, 214407 (2011). URL <https://link.aps.org/doi/10.1103/PhysRevB.83.214407>.
- [42] Ding, L., Colin, C. V., Darie, C. & Bordet, P. SrMGe_2O_6 ($M=\text{Mn,Co}$): a family of pyroxene compounds displaying multiferroicity. *J. Mater. Chem. C* **4**, 4236–4245 (2016). URL <https://doi.org/10.1039/C6TC00149A>.
- [43] Ringler, J. A., Kolesnikov, A. I. & Ross, K. A. Single-ion properties of the transverse-field Ising model material CoNb_2O_6 . *Phys. Rev. B* **105**, 224421 (2022). URL <https://link.aps.org/doi/10.1103/PhysRevB.105.224421>.
- [44] Banerjee, A., Bridges, C. A., Yan, J. Q. *et al.* Proximate kitaev quantum spin liquid behaviour in a honeycomb magnet. *Nat. Mater.* **15**, 733 (2016). URL <https://doi.org/10.1038/nmat4604>.
- [45] Lin, G., Jeong, J., Kim, C. *et al.* Field-induced quantum spin disordered state in spin-1/2 honeycomb magnet $\text{Na}_2\text{Co}_2\text{TeO}_6$. *Nat. Commun.* **12**, 5559 (2021). URL <https://doi.org/10.1038/s41467-021-25567-7>.
- [46] Liu, X. & Kee, H.-Y. Non-Kitaev versus Kitaev honeycomb cobaltates. *Phys. Rev. B* **107**, 054420 (2023). URL <https://link.aps.org/doi/10.1103/PhysRevB.107.054420>.
- [47] Streltsov, S. V. & Khomskii, D. I. Electronic structure and magnetic properties of pyroxenes (Li,Na) $\text{TM}(\text{Si,Ge})_2\text{O}_6$: Low-dimensional magnets with 90° bonds. *Phys. Rev. B* **77**, 064405 (2008). URL <https://link.aps.org/doi/10.1103/PhysRevB.77.064405>.
- [48] Feng, X.-Y., Zhang, G.-M. & Xiang, T. Topological characterization of quantum phase transitions in a spin-1/2 model. *Phys. Rev. Lett.* **98**, 087204 (2007). URL <https://link.aps.org/doi/10.1103/PhysRevLett.98.087204>.
- [49] Brzezicki, W., Dziarmaga, J. & Oleś, A. M. Quantum phase transition in the one-dimensional compass model. *Phys. Rev. B*

- 75, 134415 (2007). URL <https://link.aps.org/doi/10.1103/PhysRevB.75.134415>.
- [50] Yang, W., Nocera, A. & Affleck, I. Comprehensive study of the phase diagram of the spin- $\frac{1}{2}$ Kitaev-Heisenberg-Gamma chain. *Phys. Rev. Res.* **2**, 033268 (2020). URL <https://link.aps.org/doi/10.1103/PhysRevResearch.2.033268>.
- [51] Gallegos, C. A. & Chernyshev, A. L. Magnon interactions in the quantum paramagnetic phase of CoNb_2O_6 . *arXiv preprint arXiv:2312.03829* (2023). URL <https://arxiv.org/pdf/2312.03829>.
- [52] Chaloupka, J. & Khaliullin, G. Hidden symmetries of the extended Kitaev-Heisenberg model: Implications for the honeycomb-lattice iridates A_2IrO_3 . *Phys. Rev. B* **92**, 024413 (2015). URL <https://link.aps.org/doi/10.1103/PhysRevB.92.024413>.
- [53] Toth, S. & Lake, B. Linear spin wave theory for single-Q incommensurate magnetic structures. *J. Phys. Condens. Matter* **27**, 166002 (2015). URL <http://stacks.iop.org/0953-8984/27/i=16/a=166002>.
- [54] Songvilay, M. *et al.* Kitaev interactions in the Co honeycomb antiferromagnets $\text{Na}_3\text{Co}_2\text{SbO}_6$ and $\text{Na}_2\text{Co}_2\text{TeO}_6$. *Phys. Rev. B* **102**, 224429 (2020). URL <https://link.aps.org/doi/10.1103/PhysRevB.102.224429>.
- [55] Kim, C. *et al.* Antiferromagnetic Kitaev interaction in $J_{eff}=1/2$ cobalt honeycomb materials $\text{Na}_3\text{Co}_2\text{SbO}_6$ and $\text{Na}_2\text{Co}_2\text{TeO}_6$. *J. Phys. Condens. Matter* **34**, 045802 (2021). URL <https://doi.org/10.1088/1361-648x/ac2644>.
- [56] Samarakoon, A. M., Chen, Q., Zhou, H. & Garlea, V. O. Static and dynamic magnetic properties of honeycomb lattice antiferromagnets $\text{Na}_2\text{M}_2\text{TeO}_6$, $M = \text{Co}$ and Ni . *Phys. Rev. B* **104**, 184415 (2021). URL <https://link.aps.org/doi/10.1103/PhysRevB.104.184415>.
- [57] Sanders, A. L. *et al.* Dominant Kitaev interactions in the honeycomb materials $\text{Na}_3\text{Co}_2\text{SbO}_6$ and $\text{Na}_2\text{Co}_2\text{TeO}_6$. *Phys. Rev. B* **106**, 014413 (2022). URL <https://link.aps.org/doi/10.1103/PhysRevB.106.014413>.
- [58] Ehlers, G., Podlesnyak, A., Niedziela, J. L., Iverson, E. B. & Sokol, P. E. The new cold neutron chopper spectrometer at the Spallation Neutron Source: design and performance. *Rev. Sci. Instrum.* **82**, 085108 (2011). URL <https://doi.org/10.1063/1.3626935>.
- [59] Ehlers, G., Podlesnyak, A. & Kolesnikov, A. I. The cold neutron chopper spectrometer at the Spallation Neutron Source - A review of the first 8 years of operation. *Rev. Sci. Instrum.* **87**, 093902 (2016). URL <https://doi.org/10.1063/1.4962024>.
- [60] Granroth, G. E. *et al.* SEQUOIA: a newly operating chopper spectrometer at the SNS. *J. Phys. Conf. Ser.* **251**, 012058 (2010). URL <http://stacks.iop.org/1742-6596/251/i=1/a=012058>.
- [61] Arnold, O. *et al.* Mantid—Data analysis and visualization package for neutron scattering and μSR experiments. *Nucl. Instrum. Methods Phys. Res. A* **764**, 156–166 (2014). URL <https://www.sciencedirect.com/science/article/pii/S0168900214008729>.
- [62] Azuah, R. *et al.* DAVE: a comprehensive software suite for the reduction, visualization, and analysis of low energy neutron spectroscopic data. *J. Res. Natl. Inst. Stan. Technol.* **114**, 341 (2009). URL <https://pubmed.ncbi.nlm.nih.gov/27504233/>.
- [63] Kresse, G. & Furthmüller, J. Efficient iterative schemes for ab initio total-energy calculations using a plane-wave basis set. *Phys. Rev. B* **54**, 11169–11186 (1996). URL <https://link.aps.org/doi/10.1103/PhysRevB.54.11169>.
- [64] Perdew, J. P., Burke, K. & Ernzerhof, M. Generalized Gradient Approximation Made Simple. *Phys. Rev. Lett.* **77**, 3865–3868 (1996). URL <https://link.aps.org/doi/10.1103/PhysRevLett.77.3865>.
- [65] Blöchl, P. E. Projector augmented-wave method. *Phys. Rev. B* **50**, 17953–17979 (1994). URL <https://link.aps.org/doi/10.1103/PhysRevB.50.17953>.
- [66] Perdew, J. P., Burke, K. & Ernzerhof, M. Generalized gradient approximation made simple. *Phys. Rev. Lett.* **78**, 1396–1396 (1997). URL <https://link.aps.org/doi/10.1103/PhysRevLett.78.1396>.
- [67] Liechtenstein, A. I., Anisimov, V. I. & Zaanen, J. Density-functional theory and strong interactions: Orbital ordering in Mott-Hubbard insulators. *Phys. Rev. B* **52**, R5467–R5470 (1995). URL <https://link.aps.org/doi/10.1103/PhysRevB.52.R5467>.
- [68] Luttinger, J. M. & Tisza, L. Theory of dipole interaction in crystals. *Phys. Rev.* **70**, 954–964 (1946). URL <https://link.aps.org/doi/10.1103/PhysRev.70.954>.

ACKNOWLEDGEMENTS

The authors thank Jong Keum for assistance with X-ray measurements. We also would like to thank Sasha Chernyshev for useful discussions. Work at Oak Ridge National Laboratory (ORNL) was supported by the U.S. Department of Energy (DOE), Office of Science, Basic Energy Sciences, Materials Science and Engineering Division. This research used resources at the Spallation Neutron Source, a DOE Office of Science User Facility operated by the Oak Ridge National Laboratory. X-ray was conducted at the Center for Nanophase Materials Sciences (CNMS) (CNMS2019-R18) at ORNL, which is a DOE Office of Science User Facility. Magnetization measurements were conducted as part of a user project at the Center for Nanophase Materials Sciences (CNMS), which is a US Department of Energy, Office of Science User Facility at Oak Ridge National Laboratory. Theoretical calculations of P.A.M., A.V.U., and S.V.S. were supported by the Russian Science Foundation via project RSF 23-12-00159, A.F.G thanks to program 122021000031-8 (Flux).

AUTHOR CONTRIBUTIONS

S.V.S. and A.F.G. conceived the project. The sample synthesis and characterization were performed by G.J.R. and A.F.G. Neutron scattering experiments and data refinement were performed by A.P., A.I.K., A.M.D.S., A.F.G., A.V.U. and P.A.M. Specific heat measurements were performed by M.A.M. Magnetization measurements were performed by Z.G. and A.M.D.S. The DFT and LSWT calculations were performed by P.A.M., A.V.U. and S.V.S. The manuscript was written by P.A.M. and S.V.S. with contributions from all the authors.

COMPETING INTERESTS

The authors declare no competing interests.

ADDITIONAL INFORMATION

Supplementary Information

The online version contains Supplementary Information avail-

able at <https://doi.org/xxx.yyy.zzz>.

Correspondence and requests for materials should be addressed to P.A. Maksimov, S.V. Streltsov or A. Podlesnyak.

Supplementary Information:

Cobalt-Based Pyroxenes: A New Playground for Kitaev Physics and Ising Model Realization

Pavel A. Maksimov,^{1,2} Alexey V. Ushakov,² Andey F. Gubkin,^{2,3} Günther J. Redhammer,⁴ Stephen M. Winter,⁵ Alexander I. Kolesnikov,⁶ Antonio M. dos Santos,⁶ Zheng Gai,⁷ Michael A. McGuire,⁸ Andrey Podlesnyak,^{6,*} and Sergey V. Streltsov^{2,9,†}

¹*Bogolyubov Laboratory of Theoretical Physics, Joint Institute for Nuclear Research, Dubna, Moscow region 141980, Russia*

²*M.N. Miheev Institute of Metal Physics of Ural Branch of Russian Academy of Sciences, S. Kovalevskaya St. 18, 620990 Ekaterinburg, Russia*

³*Institute of Natural Sciences and Mathematics, Ural Federal University, Mira St. 19, 620002 Ekaterinburg, Russia*

⁴*Department of Chemistry and Physics of Materials, University of Salzburg, Jakob-Haringer-Strasse 2a, Salzburg A-5020, Austria*

⁵*Department of Physics and Center for Functional Materials, Wake Forest University, NC 27109, USA*

⁶*Neutron Scattering Division, Oak Ridge National Laboratory, Oak Ridge, TN 37831, USA*

⁷*Center for Nanophase Materials Sciences, Oak Ridge National Laboratory, Oak Ridge, TN 37831, USA*

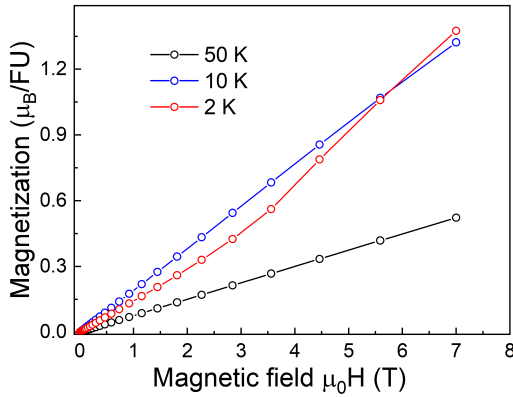
⁸*Materials Science and Technology Division, Oak Ridge National Laboratory, Oak Ridge, TN 37831, USA*

⁹*Department of Theoretical Physics and Applied Mathematics,*

Ural Federal University, Mira St. 19, 620002 Ekaterinburg, Russia

(Dated: January 25, 2024)

Supplementary Note 1: Magnetization

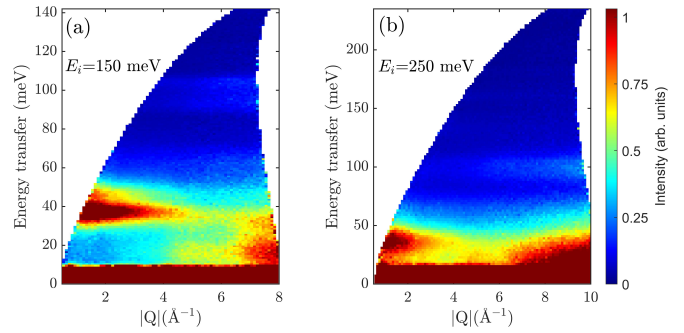


Supplementary Figure 1. Isothermal magnetization as a function of the magnetic field measured at $T = 2, 10$ and 50 K.

Supplementary Figure 1 represents isothermal magnetization curves measured below and above the Néel temperature $T_N = 9$ K. As one can see, magnetization curves measured above the Néel temperature reveal linear Brillouin-like behavior up to a magnetic field as high as 7 T. On the contrary, the magnetization curve at low temperature $T = 2$ K exhibits metamagnetic-like behavior with a critical field of $\mu_0 H_c \approx 4$ T. No sign of saturation can be observed on the $M(H)$ curve measured at $T = 2$ K in magnetic fields up to 7 T.

Supplementary Note 2: High-energy inelastic neutron scattering

Supplementary Figure 2 shows the INS spectra measured with incident energies of $E_i = 150$ meV and 250 meV. In general, phonon scattering intensity tends to increase proportionally



Supplementary Figure 2. Inelastic neutron scattering spectra taken at the SEQUOIA spectrometer at $T = 6$ K with incident neutron energies $E_i = 150$ meV (a) and $E_i = 250$ meV (b).

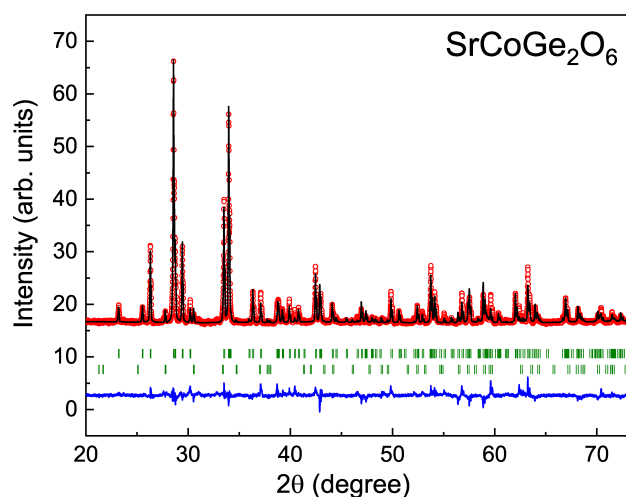
with $|Q|^2$, while CEF excitation intensity decreases with $|Q|$ following a magnetic form factor. This distinct Q -dependence behavior for phonon and CEF excitations makes it simple to distinguish between them. Both phonon and CEF excitations contribute to the spectra for energy transfers below $E_f < 60$ meV. However, above 60 meV, the INS intensity is primarily governed by lattice excitations only. Notably, an excitation band at approximately 100 meV appears at large wavevector transfers $|Q|$, consistent with phonon excitations. Regarding the CEF excitations, the expected transitions in this energy range are either too weak or too broad to be observable in the obtained spectra. This makes it challenging to distinguish them from background signals. As a result, it remains challenging to establish the complete CEF level scheme for Co^{2+} in this material.

Supplementary Note 3: X-ray diffraction

The x-ray diffraction measurements have been performed at room temperature to carry out structural characterization and to check the phase purity of the $\text{SrCoGe}_2\text{O}_6$ sample. The measurements were conducted on a PANalytical X'Pert Pro MPD equipped with an X'Celerator solid-state detector. The x-ray beam was generated at 45 kV/ 40 mA, and the wavelength was set at $\lambda = 1.5418$ Å (Cu $K\alpha$ radiation). The step

* Corresponding author: podlesnyakaa@ornl.gov

† Corresponding author: streltsov.s@gmail.com



Supplementary Figure 3. Rietveld refinement of the x-ray diffraction pattern measured at room temperature. Observed, calculated profiles and difference curves are represented by red circles, a solid black line through the symbols, and a blue line at the bottom, respectively. The first line of bars below the patterns represents Bragg peaks positions of the $\text{SrCoGe}_2\text{O}_6$ phase while the second line corresponds to the $\text{Sr}_3\text{CoGe}_5\text{O}_{14}$ impurity phase.

size was 0.016° and the exposure time at each step was 40 seconds. The Rietveld refinement has been done using the monoclinic structure model (space group $C2/c$) previously reported for $\text{SrCoGe}_2\text{O}_6$ ¹. It was found that this model well describes most of the Bragg peaks on the x-ray diffraction pattern. However, a weak contribution from the $\text{Sr}_3\text{CoGe}_5\text{O}_{14}$ impurity phase (space group $P321$) was observed on the x-ray diffraction data. The total amount of the impurity phase was estimated as 3.5% by the Rietveld refinement. The best-fit result is shown in Supplementary Figure 3. The refined unit cell parameters of the main $\text{SrCoGe}_2\text{O}_6$ phase are as follows $a = 10.2622(8)\text{\AA}$, $b = 9.2998(8)\text{\AA}$, $c = 5.4742(4)\text{\AA}$ and $\beta = 105.584(3)^\circ$.

[1] Ding, L., Colin, C. V., Darie, C. & Bordet, P. SrMGe_2O_6 (M=Mn,Co): a family of pyroxene compounds displaying multiferroicity. *J. Mater. Chem. C* **4**, 4236–4245 (2016). URL

<https://doi.org/10.1039/C6TC00149A>.